PERGAMON

International Journal of Solids and Structures 38 (2001) 3735–3757

INTERNATIONAL JOURNAL OF SOLIDS and STRUCTURES

www.elsevier.com/locate/ijsolstr

# An analytical model for stability analysis of rock layers over a circular opening

Hans H. Vaziri *, Javad S. Jalali, Rafiq Islam

*Department of Civil Engineering, Dalhousie University, 1360 Barrington Street, Halifax, Nova Scotia, Canada B3J 2X4*

Received 12 December 1999; in revised form 2 June 2000

**Abstract**

The objective of the study presented is to provide an analytical solution for determining the stability of a flexible rock layer overlying a circular opening. This problem is of general interest to the mining community but is particularly relevant to the oil and gas industry where drilling of deep wellbores often results in sand production around the well and hence opening of cavities that extend upwards until they encounter a competent caprock. One of the critical design issues in completing the wellbores is the overall stability of the formation around the well which is largely governed by the stability of the rock layer spanning over the opening. The proposed method is based on the assumption that both the caprock and the overlying soil behave plastically under compression upon reaching the yield criterion without brittle failure. It is assumed that a compression dome is formed in the caprock that carries the weight of the caprock and the overburden pressure to the surrounding soil. A plastic region in the form of a cylinder is assumed to develop above the caprock. The overburden pressure is assumed to be the minimum vertical stress between the caprock and the plastic region required for the stability of the overlying soil. The validity of the assumptions embodied in the proposed analytical model and the methodology used to develop the formulations are checked against the results obtained from a general numerical model. Despite the inherent constraints placed on most analytically-based models with respect to boundary conditions and material behaviour, the results from the proposed model show surprisingly consistent response against the numerical results. The differences between the models are rigorously discussed in this paper. The proposed method is considered to provide the designers a viable tool for solving practical problems in a cost-effective fashion. 

*Keywords:* Arching; Roof stability; Cylindrical opening; Safety factor; Excavation; Deflection; Plasticity; Finite difference

## 1. Introduction

The primary objective of the work presented here is to offer a viable tool for assessing the stability of soil/rock layer overlying a cylindrical opening created by removal of soil. Basically, a solution is sought for the roof stability which has applications to mining, geotechnical and reservoir engineering problems. It is the

* Corresponding author. Tel.: +1-902-494-3217; fax: +1-902-494-3108.
*E-mail address:* hans.vaziri@dal.ca (H.H. Vaziri).

0020-7683/01/$ - see front matter 
PII: S0020-7683(00)00239-0

latter, however, that gave the impetus for conducting the study. To provide context, it is useful to describe the physical problem and its significance.

To recover oil and gas from deep reservoirs, wellbores are drilled which may be vertical, slanted or horizontal. These wells are generally cased and perforated within the pay-zone; in some cases, however, wellbores are completed as an openhole. Drilling of wellbores results in shear failure of the formation around the hole. This often creates some instability (break out and sloughing of the material around the well face) particularly if the formation is weak and uncemented (e.g., sandy formations with very low cohesion). This failed material can be transported into the wellbore during the fluid production phase resulting in what is known as sand production. Potential for sand production increases with the rate of seepage. Production of solids results in development of cavities. The cavity grows and expands in the direction of the inflow. In the context of the work presented here involving massive sand production, cavity zone predominantly propagates upwards gravitationally rather than propagating laterally into the formation under the pressure gradient. In the field, the extent of disturbance in vertical direction is limited by the overburden caprock. If all the destabilized sands/solids are removed, the perforation cavities will grow and merge forming a large cavern.

The conventional practice followed by most oil and gas operating companies is to minimize or eliminate sand production by using liners, gravel packs and filters. Sand exclusion measures tend to compromise well's productivity as they become clogged over time. Cleaning out the screens and gravel packs are expensive and often cannot be performed effectively and, in any event, require to be applied repeatedly over the life of the well. Owing to the significant initial capital cost of completing wells with screens (which typically is in excess of $100 K but can exceed several hundreds of thousands in the case of long horizontal wells) and the maintenance and work-over costs plus the appreciable losses arising from reduced productivity, interest has been shifted towards techniques that allow sand production during the wellbore completion phase. The idea here is that by inducing sand production and facilitating its flow during the drilling phase until a stable condition is reached one can avert the situation of dealing with the more costly measures of preventing sanding during the production phase. Using this concept of creating a stable sand free condition requires having a stable roof over the cavity that is likely to be generated in the zones affected by sand removal. That means having a caprock within a close proximity of the reservoir that can span in a stable form over the cavity around the wellbore.

To aid easier understanding of the above-mentioned mechanisms leading to creation and growth of a cavity, the schematics shown in Fig. 1 may be helpful. Fig. 1(a) shows the initial stage of cavity development around a perforation. Fig. 1(b) shows the expansion of the cavity; Fig. 1(c) shows the fully developed cavity which can be considered to be a stable condition provided the caprock does not fail.

There are a number of field cases and experimental data to show that in cases where a stable cavity has been formed, sand production has been responsible for increase in productivity by several folds. Palmer et al. (1993) discuss a field project where solids production resulted in a stable enlarged cavity (average radius of about 1.4 m) around a wellbore (having an initial radius of 0.12 m) and that resulted in about three times increase in productivity. In numerical modeling of this problem, as described in Vaziri et al. (1997a), similar performance in productivity was realized. Experimental centrifuge tests described in Vaziri et al. (1997b, 1998) show that sand production results in a stable cone-shaped cavity under the caprock and the flow production improves by over 400%. Yeung (1995) described a field project where sand production in some wells improved productivity by a significant margin (as much as 10 times) but then in some areas sand production damaged the weak overlying caprock (in this shale) resulting in continuous solids production which eventually led to the suspension of the wells (once connection was made to the overlying water-bearing acquifer). This case demonstrates the importance of the role of the caprock.

The objective of the present work is to provide a simple-to-use analytical method to determine the safety factor of a given caprock against failure. To establish our analytical method, we consider the configuration shown in Fig. 2 in which a hard stratum, referred to as caprock, covers a cavity of radius b. The caprock

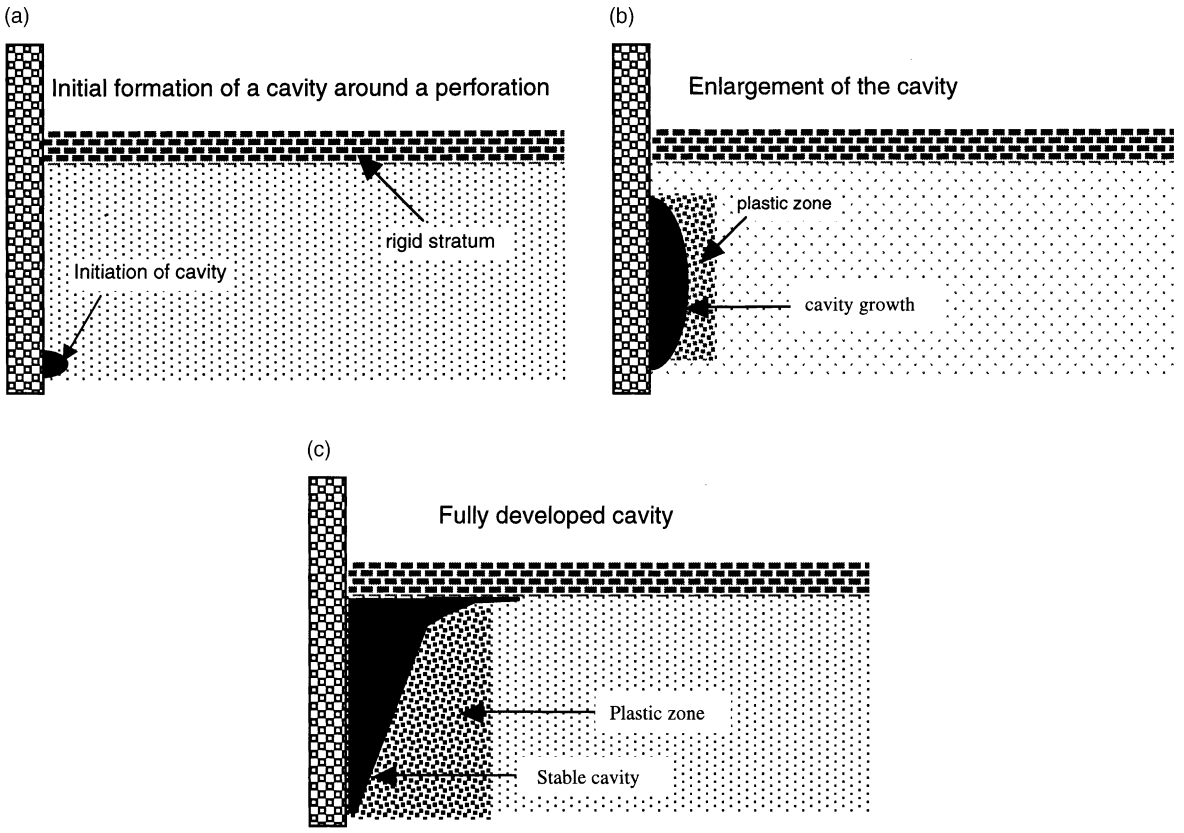


Fig. 1. Schematic illustration of sand production resulting in the development of an enlarged cavity.

behaves as a barrier against the overburden soil from falling into the cavity, and therefore we assume that it acts as a structural element for carrying its own weight and the pressure applied from the overlying soil. The problem is axisymmetric about the axis of the well.

To develop a solution, the above problem is broken into two parts: (1) estimation of the pressure transmitted to the caprock from the overlying soil, and (2) computation of the caprock response due to the applied load. These are discussed below.

## 2. Overburden pressure

Under in situ conditions, the caprock is typically under a very high stress due to the weight of the overlying material that extends from the top of the caprock to the ground surface. This stress is significantly reduced as the wellbore is drilled and the cavity is enlarged. There are a number of mechanisms that result in this pressure reduction. We introduce and discuss these mechanisms in this section and then provide a solution for predicting the overburden pressure. Throughout this section, it is assumed that the overlying soil and the caprock behave plastically under compression upon reaching the failure criterion. Moreover, we assume that the overlying soil acts like a Mohr–Coulomb material.

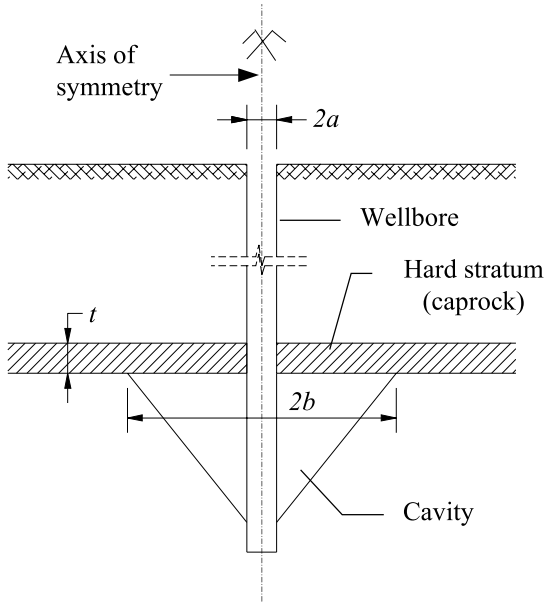


Fig. 2. Configuration of caprock and the underneath cavity.

### 2.1. Mechanisms for overburden pressure reduction

The mechanisms for overburden pressure reduction include loss of horizontal stress due to the wellbore drilling, deflection of the section of the caprock overhanging the enlarged cavity, and deformation of the soil underlying the caprock. Schematic representation of overburden reduction by means of Mohr stress circles, as a result of these mechanisms, is shown in Fig. 3. In this figure, the circle marked "1" represents the state of stresses under initial condition, and followed by the circles numbered in ascending order representing the state of the stresses at different stage of drilling and cavity growing.

Upon the creation of wellbore, the in situ horizontal stress around the wellbore lining decreases significantly. In elasto-plastic materials, vertical stress (or the overburden pressure) reduces with the horizontal stress. This phenomenon as schematically illustrated in Fig. 3 starts from circle 1. At this stage, as the Mohr circle is below the failure envelope, the soil behavior is governed by its stress–strain relationship. With the decrease of $\sigma_{hr}$ (the radial horizontal stress) Mohr circle enlarges until it touches the failure envelope (circle 2). After this stage, reduction of $\sigma_{hr}$ is not possible unless $\sigma_v$ reduces in such a way that the corresponding Mohr circle remains tangent to the failure envelope. As a result, a plastic region is created

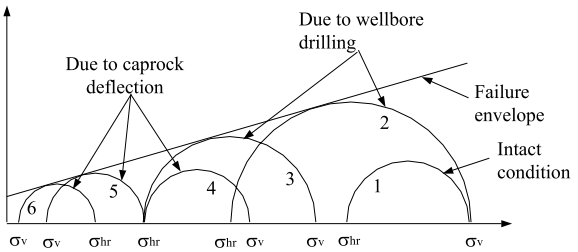


Fig. 3. Successive stress reduction due to wellbore drilling and caprock deflection.

around the well wherein all the three principal stresses decrease as the distance from the well lining becomes smaller. For a complete discussion of this subject, reference can be made to Florence and Schwer (1978), Risnes et al. (1982) and Wang and Dusseault (1994).

Overburden reduction as a result of caprock increasing deflection (due to the cavity enlargement) follows the stress reduction due to the drilling. As the cavity grows, the overburden pressure drops (circle 4) until it becomes smaller than the horizontal stress; continuation of this state, as represented by circle 5, results in the overburden soil yielding. As the overburden pressure on the caprock decreases, arching action transmits the weight of the upper soil to the neighboring region. This reduction eventually creates a plastic region above the caprock. The stress in the plastic region decreases in such a manner that the corresponding Mohr circle remains tangent to the failure envelope (circles 5 and 6 in Fig. 3). Reduction of the overburden pressure continues until an unstable state develops.

As the cavity enlarges, the underlying soil will tend to settle in response to both the stress increase in this region and the soil movement towards the cavity once it becomes plastic. This settlement adds to the caprock deflection leading to a reduction in the overburden pressure.

### 2.2. Soil–caprock interaction diagram

The concept of overburden reduction can be explained better by the soil–caprock interaction diagram shown in Fig. 4. In this figure, the curve abcd represents the behavior of the overlying soil versus deflection of the caprock. This curve starts from the at-rest condition (point a) and ends on line cd where the magnitude of overburden pressure has reached its minimum value for maintaining a stable condition. The states of stresses corresponding to points a and b are represented by circles 3 and 5 in Fig. 3, respectively. Curves denoted by numbers represent different characteristics such as the caprock thickness, the opening diameter and the material constitutive relationship. The intersection point of each caprock curve with the soil curve determines the magnitude of the overburden pressure and the deflection for the given caprock.

In Fig. 4, curve 1 represents a very stiff caprock that intersects curve abcd in its elastic range. As the figure shows, the magnitude of overburden pressure is close to the at-rest condition. This situation usually exists when the diameter of the cavity is small. When the diameter of the cavity increases, the caprock becomes more flexible, and therefore, it intersects curve abcd at a smaller value of overburden pressure. This situation is represented by curve 2. The enlargement of the cavity can continue until the situation shown by curve 3 occurs. At this stage, the caprock is on the verge of failure and no further cavity

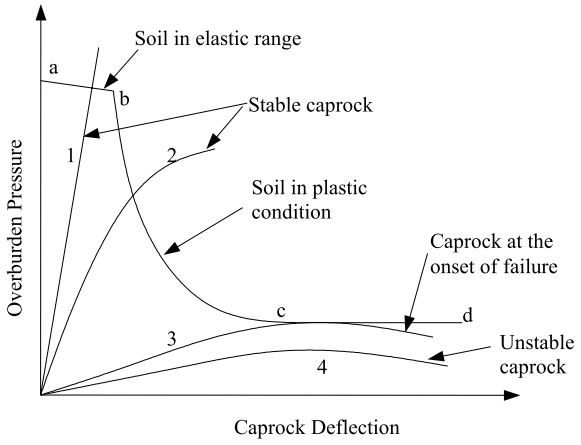


Fig. 4. Soil and caprock interaction diagram.

enlargement can be tolerated. Curve 4 does not intersect curve abcd and therefore, represents an unstable condition. This curve represents a caprock underlain by a cavity size under which the caprock cannot sustain the minimum overburden pressure.

### 2.3. Determination of overburden pressure

The overburden pressure considered in this section is the minimum needed for the stability of the overlying soil represented by line cd in Fig. 4. To determine this pressure, we consider a plastic region above the caprock in the form of a cylinder having the same diameter as the cavity. This idealization is shown in Fig. 5. The stress at the bottom of this region is equal to the overburden pressure applied to the caprock. The soil above the region is in elastic condition. Therefore, referring to Fig. 3, the stress at the top of the region is equal to $\sigma_v$ of circle 5. We consider a thin horizontal element of height $\mathrm{d}z$ at elevation $z$ above the caprock. The forces acting on this element are $\pi b^2(\sigma_z + \mathrm{d}\sigma_z)$, vertical force along the top of the element, $\pi b^2\sigma_z$, vertical force along the bottom of the element, $W = \gamma\pi b^2\mathrm{d}z$, weight of the element, and $2\pi b\tau\,\mathrm{d}z$, upward shear force acting around the circumference of the element.

Assuming a cohesionless soil, the upward shear stress acting around the circumference ($\tau$) can be expressed by

$$\tau = \sigma_h \tan\phi, \tag{1}$$

where

$$\sigma_h = \sigma_z K_{\mathrm{act}} \tag{2}$$

and

$$K_{\mathrm{act}} = \tan^2\left(45 - \frac{\phi}{2}\right). \tag{3}$$

Equilibrium of the forces in the vertical direction requires

$$\pi b^2(\sigma_z + \mathrm{d}\sigma_z) + \gamma\pi b^2\mathrm{d}z = b\pi^2\sigma_z + 2\pi b(\sigma_z K_{\mathrm{act}})\tan\phi\,\mathrm{d}z, \tag{4}$$

which after simplification becomes

$$\mathrm{d}z = \frac{\mathrm{d}\sigma_z}{m\sigma_z - \gamma}, \tag{5}$$

where

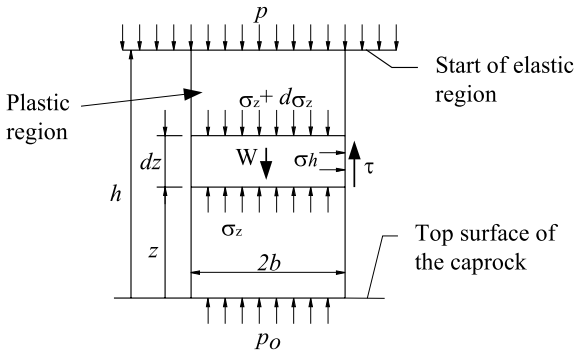


Fig. 5. Idealization used for the determination of overburden pressure.

$$m = \frac{2}{b} K_{\text{act}} \tan\phi. \tag{6}$$

Integrating Eq. (5) from $z = 0$ to $z = h$, yields

$$h = \frac{1}{m} \ln \frac{mp - \gamma}{mp_0 - \gamma}. \tag{7}$$

With some manipulation, we can write Eq. (7) in the following form:

$$p_0 = \frac{mp - \gamma}{me^{mh}} + \frac{\gamma}{m}. \tag{8}$$

Eq. (7) shows that when $p_0$ decreases, the height of the plastic region increases. Eq. (8) also shows that as the height of the plastic region becomes large, the effect of the first term in the equation becomes insignificant and, therefore, the value of $p_0$ approaches the minimum value of $\gamma/m$. According to our assumption regarding the plastic behavior of the soil and the caprock, the minimum value of $p_0$ is the overburden pressure at the onset of the caprock failure.

To clarify the above better, let us consider a situation where the overburden pressure is more than the minimum value and the caprock is deflecting plastically under the applied load. If the applied load remains constant the caprock will fail. However, as the deflection of the caprock increases, larger region above the caprock becomes plastic and as a result the overburden pressure decreases. Due to this reduction of the overburden pressure, the caprock stops deflecting and failure is averted.

Substituting the value of $m$ from Eq. (6) into the expression for the minimum $p_0$ yields the following expression for the overburden pressure at the onset of the caprock failure

$$p_0 = \frac{\gamma}{m} = \frac{\gamma b}{2K_{\text{act}} \tan\phi}. \tag{9}$$

It is important to mention that Eqs. (1) and (2) are consistent with the assumption of Spangler and Handy (1971) for calculating the overburden pressure for pipes. Meyerhof and Adams (1968) also used similar assumption to determine the bearing capacity of foundations with tension forces. Nevertheless, these equations technically are not correct. That is because, the relationship between the vertical stress and the horizontal stress expressed by Eq. (2) is for the situations where these stresses are the principal stresses, while Eq. (1) is valid if the vertical plane is a plane of failure. For a Mohr–Coulomb material these two conditions cannot exist simultaneously. Moreover, based on Eq. (2), the horizontal stress is less than the vertical stress. This does not follow the expected soil behavior as depicted in Fig. 3. To overcome these inconsistencies we modify the above solution assuming that the vertical plane makes an angle $\alpha$ with the minor principle plane. This modified solution is discussed below.

### *2.3.1. Modified solution*

Fig. 6 shows the Mohr stress circle for the soil in plastic region above the caprock, in which $\sigma_h$ and $\sigma_z$ are the horizontal and vertical stresses, respectively, and $\sigma_1$ and $\sigma_3$ are the principal stresses. According to this figure, the following relationship is obtained for the shear stress at the vertical side of the plastic region in Fig. 5.

$$\tau = \frac{\sigma_z \sin\phi \sin 2\alpha}{1 - \sin\phi \cos 2\alpha}. \tag{10}$$

Substituting this equation into Eq. (4) to replace $(\sigma_z K_{\text{act}}) \tan\phi$ and repeating the remaining operations yields

$$p_0 = \frac{\gamma}{m}, \tag{11}$$

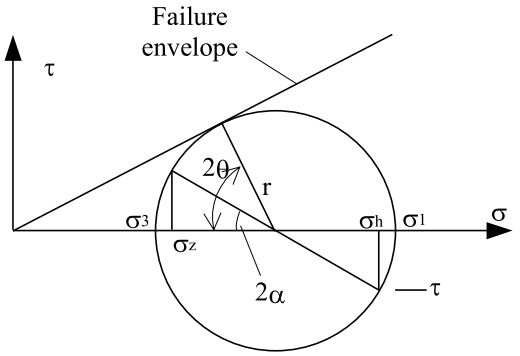


Fig. 6. Mohr's circle for the state of stresses in the plastic zone.

where

$$m = \frac{2\sin\phi\sin 2\alpha}{b(1-\sin\phi\cos 2\alpha)}. \tag{12}$$

One can obtain the maximum and minimum values of $P_0$ by setting the derivative of Eq. (12) with respect to $\alpha$ equal to zero. The maximum value of $P_0$ is infinity which occurs for $\alpha = 0$. The minimum value of $p_0$ is obtained for $\alpha = \theta = \phi/2 - 45^\circ$. Considering the fact that $\alpha$ is not constant along the whole depth of the plastic region, we assume that it varies from $\alpha = \phi/2 - 45^\circ$ at the bottom of the region to $\alpha = 0$ at the top. Therefore, the average value of $\alpha$ within the region is less than $\alpha = \phi/2 - 45^\circ$ and can be expressed as

$$\alpha_{avr} = \frac{\phi/2 - 45^\circ}{S}, \tag{13}$$

where $S$ is larger than 1. Our numerical studies using finite difference models show that the $S$ value changes as a function of $\phi$. Its value for larger $\phi$ is smaller than for smaller $\phi$. However, a value of $S = 10$ has shown to provide acceptable results for the common range of $\phi$ in practice. Assuming $S = 10$ and substituting Eqs. (12) and (13) in Eq. (11) yields

$$p_0 = \frac{b}{2}\left[\frac{\gamma\sin\phi\sin(\phi/10 - 9^\circ)}{1-\sin\phi\cos(\phi/10 - 9^\circ)}\right]. \tag{14}$$

To illustrate the changes arising from the above modifications, Fig. 7 shows plots of Eqs. (9) and (14) for $b = 2$ m. Based on general understanding from soil behavior, one expects that the overburden pressure

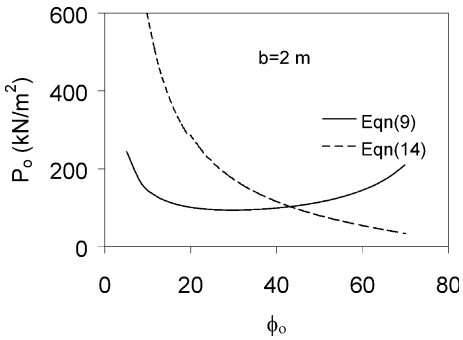


Fig. 7. Comparison of Eqs. (9) and (14).

should decrease as the value of $\phi$ increases. The behavior of Eq. (14), as shown in Fig. 7, is compatible with this expectation. However, Eq. (9) reaches a minimum value for $\phi = 30^\circ$ which cannot be realistic. Therefore, it is recommended that Eq. (14) be used in practice. Nevertheless, it is important to mention that the two equations provide similar results for $\phi \approx 40^\circ$. Since the friction angles commonly obtained for soils overlying the caprocks are close to this value, from a practical point of view, the difference of the two equations is not generally significant.

## 3. Behavior of caprock

To adopt a theory to explain the behavior of a caprock, we resort to the available solutions for the stability of openings' roofs in mining related applications. This problem has been discussed thoroughly in the literature and various solutions have been suggested. For example, the reader may refer to Adler and Sun (1968), Baker and Hatt (1972) and Sterling (1980). One of the solutions that is commonly used in practice (Obert and Duvall, 1967) assumes that the caprock is a flexural element and it fails when the stress at the extreme top or bottom fiber of a critical section exceeds the tensile strength of the material.

Another practical method for assessing an opening's roof stability is the one proposed by Evans (1941) which was later modified and extended by Beer and Meek (1982). According to this method, the stability of the roof layer is not limited to the rock tensile strength. This is due to the fact that after the development of tension cracks, the roof consists of a number of separated blocks that will remain stable as a result of compressive force acting between them. Therefore, the roof stability is governed by the rock's compressive strength. This concept is shown in Fig. 8 for a long opening in a stratified rock.

We adopt Beer and Meek's concept to develop a solution for the caprock problem. We assume that the caprock is comprised of a material that is elasto-plastic under compression and has no tensile strength. While the assumption of no tensile strength is conservative it is considered to be a valid one in most field cases involving flexible, ductile caprocks like shales. Most weak and friable rocks have a much smaller tensile strength (almost negligible) than those reported based on the assumption of a linear failure envelope (Vaziri et al., 1997c). We consider a circular plate that has a central hole and extends into the soil beyond the cavity. It carries the applied overburden pressure and its own weight and transfers these to the soil around the cavity. When this plate is subjected to a vertical load, tensile stresses are produced at the bottom of the plate in its central part as well as at the top of the plate in the region close to the support. As the caprock is considered to have zero tensile strength it cannot carry any tensile stresses. Therefore, the caprock in the tensile region cracks and a compression dome forms in the caprock. With the enlargement of the cavity, the depth of the cracked region increases and the compression stress in the compression dome

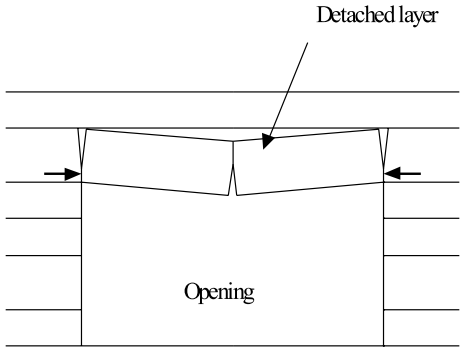


Fig. 8. Stability of an opening's roof after development of tension cracks.

becomes larger. Yielding of the caprock material in the compression dome starts from extreme fiber in compression and gradually continues towards the inner side. Failure occurs when one circular section becomes completely plastic.

Fig. 9 illustrates the configuration of the compression dome in the caprock at the onset of failure. The dome is axisymmetric about the axis of the wellbore and is assumed to be parabolic in shape in the vertical plane passing through the axis of symmetry. Caprock's thickness is assumed constant. Fig. 10 shows the centerline (meridian curve) of the dome and the adopted coordinate system. The meridian is a parabola and its shape can be expressed by

$$y = \frac{z}{b^2}x^2. \tag{15}$$

Therefore,

$$y' = \frac{2z}{b^2}x \tag{16}$$

$$y'' = \frac{2z}{b^2} \tag{17}$$

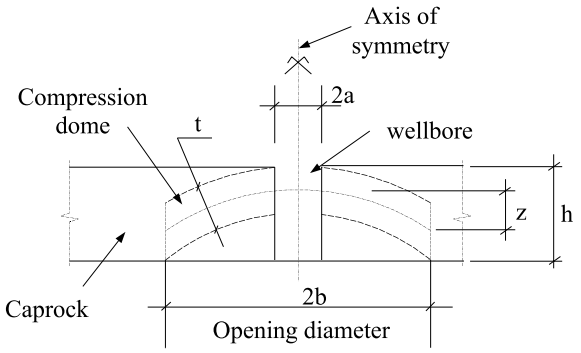


Fig. 9. The schematic of the compression dome within the caprock.

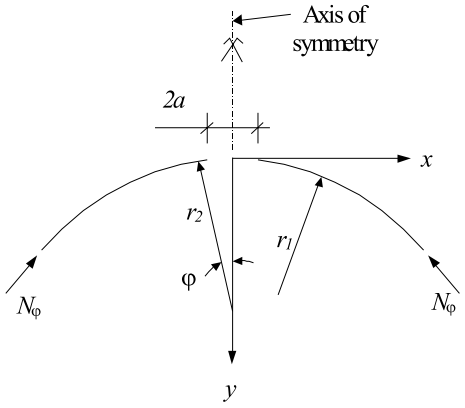


Fig. 10. Meridian of the compression dome.

and

$$\varphi = Atn(y'). \tag{18}$$

Radius of curvature of the meridian curve is

$$r_1 = \frac{\left(1+y'^2\right)^{3/2}}{y''} = \frac{b^2}{2z}\left(1+\frac{4z^2}{b^4}x^2\right)^{3/2}. \tag{19}$$

The dome is generated by the revolution of the meridian about the $y$-axis. The radius of revolution as defined in Fig. 10 is

$$r_2 = \frac{x}{\sin\varphi}. \tag{20}$$

The radial force at a radius equal to $x$ from the origin is expressed by

$$N_\varphi = \frac{F}{2\pi x \sin\varphi}, \tag{21}$$

where $F$ represents the resultant of the load applied above the section under consideration. The reader can find the proof of this equation in a number of books including Timoshenko (1940) and Ugural (1981). For the present case, $F$ can be expressed as

$$F = \pi q(x^2 - a^2), \tag{22}$$

therefore,

$$N_\phi = q\frac{(x^2-a^2)}{2x\sin\varphi}. \tag{23}$$

The following relationship exists between the radial ($N_\varphi$) and tangential forces ($N_\theta$),

$$\frac{N_\varphi}{r_1} + \frac{N_\theta}{r_2} = \bar{p}, \tag{24}$$

where $\bar{p}$ is the component of the applied load in terms of pressure perpendicular to the surface of the dome, i.e.,

$$\bar{p} = q\cos^2\varphi. \tag{25}$$

Substituting Eqs. (19)–(23) and Eq. (25) into Eq. (24) yields

$$N_\theta = q\left[\frac{x\cos^2\varphi}{\sin\varphi} - \frac{z(x^2-a^2)}{b^2\sin^2\varphi\left(1+\frac{4z^2}{b^4}x^2\right)^{3/2}}\right]. \tag{26}$$

Investigating Eqs. (23) and (26) reveals that both values of $N_\theta$ and $N_\varphi$ are positive and the maximum values occur at $x = a$ and $x = b$, respectively. Therefore,

$$(\sigma_\theta)_{\max} = \frac{qa\cos^2\varphi_a}{t\sin\varphi_a}, \tag{27}$$

$$(\sigma_\phi)_{\max} = \frac{q(b^2-a^2)}{2bt\sin\phi_b}. \tag{28}$$

Considering the fact that the bottom surface of the dome is facing the free space, the smallest principal stress, $\sigma_3$, is equal to zero for the whole dome. Therefore, failure can be either due to $(\sigma_\theta)_{\max}$ at $x = a$ or due

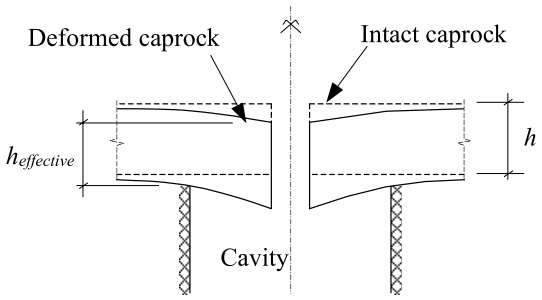


Fig. 11. Reduction of the caprock effective depth due to excessive deflection.

to $(\sigma_\varphi)_{\max}$ at $x = b$. However, as Eqs. (27) and (28) show, the magnitude of the stresses is a function of the dome geometry which is not known in advance. The following relationship holds between the various dimensions of the dome:

$$h = z + \frac{t}{2\cos\varphi_a} + \frac{t}{2\cos\varphi_b} - y_a, \tag{29}$$

where $h$ is the thickness of the caprock and $z$ the height of the dome. The geometry of the dome is defined in such a way that the strength of the dome becomes maximum. This is accomplished by using Eqs. (27)–(29) using a trial-and-error process.

It is important to note that the above solution is based on the assumption that the deformation of the caprock resulting from the applied load is small. This assumption, however, may not be correct in practice as a significant amount of deformation may be necessary for the overburden pressure to reach its minimum value. To account for this and avoid the associated problem of overestimating the caprock strength, some allowance must be made for the thickness of the caprock. Fig. 11 illustrates this point where the caprock deformation reduces the effective thickness that is considered for the solution presented in this section.

## 4. Failure criteria and safety factor

To determine the factor of safety for the caprock against failure, the failure criterion for the material must be defined. The two common failure criteria for geomechanical applications are the Mohr–Coulomb and Hoek–Brown (1980). According to these, the onset of failure (or the start of plasticity) for a given set of strength properties depends only on the values of the major and minor principal stresses. For the solution presented in Section 3, two of the principal stresses (the radial and tangential) are compressive and constant through the thickness of the dome. The third principal stress is zero as the bottom of the dome faces the cavity. Therefore, the major principal stress is the larger value obtained from Eqs. (27) and (28) while the minor one remains zero. This condition is equivalent to a uniaxialy stressed material wherein failure occurs as the applied stress reaches the unconfined compression strength of the material. Considering this fact, we define the safety factor as the ratio of the unconfined compressive strength to the maximum compressive stress in the caprock, i.e.

$$SF = \frac{q_u}{(\sigma_\varphi)_{\max} \text{ or } (\sigma_\theta)_{\max}}. \tag{30}$$

The unconfined compressive strength ($q_u$) can be obtained directly by performing unconfined compression test. However, for a Mohr–Coulomb material it can be determined indirectly from the cohesion, $c$, and the friction angle of the caprock, $\phi$, using the following relationship:

$$q_u = \frac{2c\cos\phi}{1-\sin\phi}. \tag{31}$$

## 5. Verification

To verify the proposed analytical method we analyze a number of finite difference models by using the commercial finite difference FLAC (1996) program. In this section, we present the results of these analyses and compare the results with those obtained from the proposed analytical solution.

The FLAC is an explicit finite difference program and is based on the method presented by Wilkins (1964) for deriving difference equations for nonrectangular grids. FLAC uses an explicit time-marching method to solve the problems. This means that even for finding the static solution of a problem, the dynamic equations of motion are included in the formulation. This is beneficial since the solution always remains stable, even when the physical system that is being modeled is unstable (upon collapse of a part of the system the solution can still continue).

### 5.1. FLAC model

Fig. 12 shows the configuration of the mesh considered for the FLAC models. The models simulate a cylinder 24 m in height and 12.75 m in radius; the $z$-axis is the axis of symmetry. Because of the axisymmetric nature, the problem becomes two-dimensional. The model, as shown in the figure, is divided into four horizontal and three vertical strips within which rectangular elements with different sizes are located. The height of the elements in strip II is 50 mm. This strip is used to simulate the caprock. The height of the elements above and below strip II grows gradually from 50 to 250 mm. In a similar manner the width of the elements is varied from 50 to 250 mm; elements' width in strip A is 50 mm and is gradually changed to 250 mm in strip B. The 0.1 m space between the $z$-axis and the mesh simulates the wellbore. The initial boundary conditions are $U_x = 0$ at $x = 0.1$ and 12.75 m, $U_z = 0$ at $z = 0$, $\sigma_z = p$ at $z = 24$ m, where $U_x$ and $U_z$ are the displacements in the $x$ and $z$ directions, respectively, and $p$ is the in situ vertical stress in the soil.

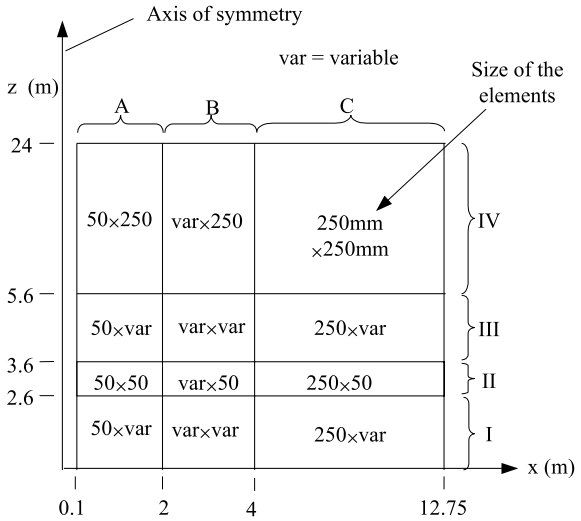


Fig. 12. Configuration of the finite difference mesh used in FLAC.

Several thousand steps are required to reach static equilibrium for the above conditions. To assure that the model stays elastic during this procedure high strength properties are used for the soil and the caprock. Upon reaching the static equilibrium the correct strength properties are assigned to the model.

To simulate the creation and enlargement of the cavity, first we release the applied constraints at $x = 0.1$ from $z = 0$ to the top of the caprock and allow FLAC to reach equilibrium. Then the soil in strip I is removed in vertical columns starting from $x = 0.1$. As every change produces a dynamic response in the model, the applied change must be applied in small increments to prevent unrealistic irreversible nonlinear behavior in the model. Small increments in the context of the problem under consideration means removal of one or two columns of grids at each stage. Removal of the soil underlying the caprock continues until failure is detected. Definition of failure in the analyses performed is explained below.

When the cavity enlarges, some of the elements at the bottom of the caprock fail in tension. This situation is equivalent to having tension crack in reality. FLAC sets the stiffness of the cracked elements to zero. As such, these elements start flowing in the solution under their own mass. This is equivalent to having the cracked material detached from the rest of the caprock. While this behavior may be somewhat realistic, it is more conservative to assume that the total weight of the cracked material is carried by the rest of the caprock. Moreover, this is consistent with our analytical solution which does not consider any weight reduction for the cracked part of the caprock. Therefore, the cracked elements in the FLAC analysis are removed and their mass is added to the caprock elements located above them. Failure is the condition when the removal of the cracked elements break through the top of the caprock, or when the program fails to reach static equilibrium. The latter case occurs when a large area of caprock fails resulting in the flow of this part of the caprock and the overlying soil into the cavity. This form of failure is illustrated in Fig. 13.

### 5.1.1. Boundary conditions

As the problem to be analyzed forms a small part of the real problem, considerations must be given to ensure that the critical boundary conditions are correctly assigned. For example, two choices are available for the boundary condition at the top-end of the model ($z = 24$ m) after creating the in situ condition: (1) imposing a fixed boundary, or (2) maintaining the existing stress boundary. If the dimension of the model is sufficiently large, the differences between these two approaches disappear. Otherwise, in general, a fixed

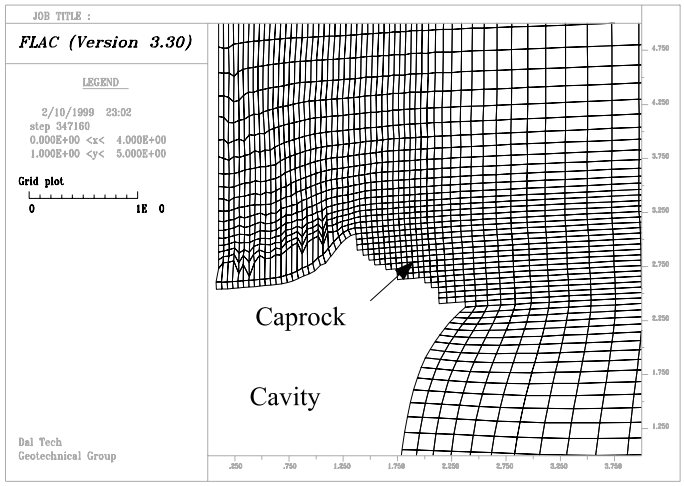


Fig. 13. Caprock failure in FLAC model.

boundary underestimates both the stresses and the displacements while a stress boundary condition tends to do the reverse.

A stress boundary condition is adopted for the top-end of the model to avoid underestimating the stresses and the displacements. As the height of the soil considered above the caprock in the model is relatively large, it is expected that the assumed boundary condition yields a reasonable representation of the real situation. To test the validity of the assumptions made, we analyzed one of the cases considered in Section 5.2 under the two different types of boundary conditions and we found the differences to be negligible.

Boundary conditions to represent the wellbore are more complicated. Right after the well opening is formed, horizontal stress becomes zero, however, this stress is partly recovered as the well casing is inserted and later as the soil moves towards the opening (creep behavior). The interaction between the soil and the well casing increases the complexity. To minimize these complexities we consider only the two extreme cases: (1) a stress-free boundary, and (2) a fixed boundary in the $x$ direction. We consider the former to be more representative as the magnitude of the recovered stress is quite small relative to the in situ stress. The latter is rather conservative as it prevents any reduction in the overburden pressure due to the removal of the horizontal stress (Section 2.1). Based on the foregoing, we assign a free boundary condition for the caprock and a fixed condition for the overlying soil.

### 5.2. Case studies

In this section, we use the proposed analytical method to calculate the radius of the cavity at the onset of failure ($SF = 1$) for four cases and compare the results against FLAC. For all cases, we assume that both the caprock and the soil behave as Mohr–Coulomb materials and the overlying soil is cohesionless. As in FLAC simulations, the cavity is created by removing the soil, in vertical strips, beneath the caprock, failure may occur in this part of the model sooner than the caprock itself. To prevent this premature failure, we assign a small amount of cohesion ($c = 20$ kPa) to the soil underlying the caprock which is also quite realistic for most weak reservoirs. The other properties of the soil above and below the caprock are considered to be the same. The wellbore radius in all cases is 0.1 m, and the following properties are common.

*Caprock:*

$$\gamma = 22 \text{ kN/m}^3,$$
$$E = 5000 \text{ MPa (used only for FLAC analysis)},$$
$$\nu = 0.3 \text{ (used only for FLAC analysis)},$$
$$\phi = 35^\circ.$$

*Soil:*

$$\gamma = 18 \text{ kN/m}^3.$$

The other properties are presented in Table 1. It is to be noted that some of the variables shown in this table, namely the soil elastic properties and the in situ vertical stress, do not play a role in the proposed analytical model. Consequently, a single cavity radius is obtained from the analytical method for each case. In FLAC, the elastic properties and vertical stress have an influence on the radius of cavity at the onset of failure.

Tables 2–5 summarize the results of the analytical method and the FLAC analyses. In these tables, column 5 is the cavity radius obtained from the analytical method based on the caprock actual thickness. The analytically-derived cavity radii shown in column 7 are based on the reduced thickness. The thickness used for this calculation is the effective thickness (Fig. 11) at the onset of failure obtained from the FLAC analysis. This value is presented in column 4. Column 6 is the cavity radius obtained from the FLAC

Table 1
Properties of soils and caprocks for case studies

| Case | Caprock | | Soil | | | |
|---|---|---|---|---|---|---|
| | Thickness (m) | $c$ (kPa) | $E^a$ (MPa) | $\nu^a$ | $\phi$ (degree) | $P^a$ (MPa) |
| 1 | 0.8 | 400 | 100, 1000 | 0.25 | 35 | 5, 20 |
| 2 | 0.8 | 400 | 100, 200, 1000 | 0.35 | 25 | 5, 20 |
| 3 | 0.8 | 400 | 100, 1000 | 0.25 | 45 | 5, 20 |
| 4 | 1.0 | 100 | 100, 1000 | 0.25 | 35 | 5, 20 |

[a] Used only for FLAC analysis.

Table 2
Results of the analyses for Case 1

| FLAC analysis | $E_{soil}$ (MPa) | $p$ (MPa) | $h_{failure}$ (m) | Radius of the cavity at the onset of failure (m) | | |
|---|---|---|---|---|---|---|
| | | | | Analytical ($h = 0.8$ m) | FLAC | Analytical ($h = h_{failure}$) |
| A | 100 | 5 | 0.66 | 1.81 | 2.19–2.27 | 1.60 |
| B | 100 | 20 | 0.55 | 1.81 | 1.5–1.55 | 1.42 |
| C | 1000 | 5 | 0.79 | 1.81 | 2.12–2.19 | 1.79 |
| D | 1000 | 20 | 0.72 | 1.81 | 2.06–2.12 | 1.69 |

Table 3
Results of the analyses for Case 2

| FLAC analysis | $E_{soil}$ (MPa) | $p$ (MPa) | $h_{failure}$ (m) | Radius of the cavity at the onset of failure (m) | | |
|---|---|---|---|---|---|---|
| | | | | Analytical ($h = 0.8$ m) | FLAC | Analytical ($h = h_{failure}$) |
| A | 100 | 5 | 0.66 | 1.57 | 1.85–1.90 | 1.39 |
| B | 100 | 20 | 0.46 | 1.57 | 1.2–1.25 | 1.1 |
| C | 200 | 20 | – | 1.57 | 1.25–1.3 | – |
| D | 1000 | 5 | 0.79 | 1.57 | 1.85–1.90 | 1.56 |
| E | 1000 | 20 | 0.78 | 1.57 | 1.5–1.55 | 1.55 |

Table 4
Results of the analyses for Case 3

| FLAC analysis | $E_{soil}$ (MPa) | $p$ (MPa) | $h_{failure}$ (m) | Radius of the cavity at the onset of failure (m) | | |
|---|---|---|---|---|---|---|
| | | | | Analytical ($h = 0.8$ m) | FLAC | Analytical ($h = h_{failure}$) |
| A | 100 | 5 | 0.69 | 2.03 | 2.27–2.36 | 1.85 |
| B | 100 | 20 | 0.57 | 2.03 | 1.55–1.6 | 1.64 |
| C | 200 | 20 | 0.71 | 2.03 | 1.9–1.95 | 1.88 |
| D | 1000 | 5 | 0.79 | 2.03 | 2.69–2.82 | 2.02 |
| E | 1000 | 20 | 0.79 | 2.03 | 2.36–2.47 | 2.02 |

Table 5
Results of the analyses for Case 4

| FLAC analysis | $E_{soil}$ (MPa) | $p$ (MPa) | $h_{failure}$ (m) | Radius of the cavity at the onset of failure (m) | | |
|---|---|---|---|---|---|---|
| | | | | Analytical ($h = 1$ m) | FLAC | Analytical ($h = h_{failure}$) |
| A | 100 | 5 | 0.95 | 1.25 | 1.45–1.5 | 1.21 |
| B | 100 | 20 | 0.72 | 1.25 | 1.25–1.30 | 1.02 |
| C | 1000 | 5 | 1 | 1.25 | 1.5–1.55 | 1.25 |
| D | 1000 | 20 | 1 | 1.25 | 1.5–1.55 | 1.25 |

analysis. This value is reported as a range between the radius of the cavity for the stage when the failure is detected and the stage before failure. Because of the stepwise enlarging of the cavity size in the FLAC analysis, the actual failure radius falls within the reported range.

### 5.2.1. Discussion of results

*5.2.1.1. General assessment of the results.* The values obtained for the radius of cavity from the FLAC analyses show that the radius of cavity is not significantly influenced by the variations in in situ vertical stress and soil elastic moduli. In general, the cavity radius is larger for stiffer overlying soil and smaller for in situ vertical stress. It is to be noted that in all cases analyzed, a significant portion of the material that had undergone tensile failure was removed from the bottom of the caprock. This removal process was gradual as the cavity was being enlarged. The profile of the caprock bottom surface at the onset of failure followed a parabolic shape, which is consistent with our assumption for the formation of a compression dome in the caprock.

The radius from the analytical method for each case is within ±25% of the values obtained from FLAC. Considering the many uncertainties involved in most geomechanical problems, this difference is considered to be well within the acceptable range for practical purposes. This is especially true when the accuracy of the present analytical method is compared with the other analytical solutions commonly used in geomechanical applications. As the results show, the analytical solutions are generally on the conservative side. However, for situations where an appreciable caprock deformation occurs before failure, the analytical method overestimates the size of the cavity. This shortfall is basically due to the caprock effective thickness reduction resulting from excessive deformation (Fig. 11) which, as was described in Section 3, can be corrected by considering a reduced thickness. The values calculated based on this consideration are reported in the last column of Tables 2–5. These values are generally equal or smaller than FLAC's.

Another reason for the smaller values of the cavity radii from the FLAC analyses can be attributed to the existence of the $x$-direction constraint in the FLAC models at the wellbore lining in the overlying soil. In practice, the boundary condition at the wellbore lining is closer to a stress-free surface than a fully fixed one. However, as mentioned earlier, the latter condition yields a conservative solution. In view of the results in Tables 2–5, it can be seen that for situations where the in situ vertical stress is high and the overlying soil soft, the predicted cavity radius from FLAC is smaller than the analytical model. These conditions require a relatively large level of caprock deflection to fully reduce the overburden pressure. As is shown in Section 5.2.1.2, in neither of these conditions the complete reduction of the overburden pressure occurred. In light of this, had the boundary condition at the wellbore lining set to a stress-free condition in the FLAC models, the overburden pressure would have become smaller resulting in a larger cavity radius.

To assess the practical significance of the underestimation in the cavity radius using the analytical model, we calculate the radii of the cavity from the analytical method for different safety factors assuming no thickness reduction. These values are presented in Table 6. As shown, when the safety factor is larger than 2, the analytical results are consistently smaller than the numerical ones.

Table 6
Radius of cavity obtained from the analytical method for different safety factors with no thickness reduction

| Case | Radius (m) | | |
|---|---|---|---|
| | SF = 1 | SF = 2 | SF = 3 |
| 1 | 1.81 | 1.41 | 1.21 |
| 2 | 1.57 | 1.23 | 1.05 |
| 3 | 2.03 | 1.58 | 1.36 |
| 4 | 1.25 | 0.95 | 0.81 |

*5.2.1.2. Variation of overburden pressure with the cavity radius*. To extend verification of the proposed analytical model, we recorded the reduction of the overburden pressure with the growth of the cavity radius in FLAC. Fig. 14 illustrates the variation of the overburden pressure for 6 points at the top of the caprock in Models A and B of Case 4. In this figure, P-1–P-6 represent a set of elements away from the well lining; P-1 is the first element immediately behind the well. It can be observed that the overburden reduction curves are similar to the curve abcd in Fig. 4. The sharp reduction of the stress for P-1 at the beginning of the curves is due to loss of horizontal stress at the well lining when the $x$-direction constraint up to the top of the caprock is removed.

To demonstrate the effect of the various factors not considered in the analytical method on the reduction of the overburden pressure, the overburden pressure curves of point P-3 from all the models considered for Case 4 are plotted in Fig. 15. In this figure, curve E represents a model similar to Model D wherein a stress-free boundary is used for the overlying soil at the wellbore lining. Note that in the other models the $x$-direction movement for the overlying soil at the well lining is restrained. As the figure shows, the overburden pressure drops faster in stiff soils than in soft soils. The curves corresponding to smaller in situ vertical stress fall below the curves for higher values. The loss of horizontal stress at the well lining also accelerates the overburden pressure reduction. Notwithstanding this, for all the cases, the overburden pressures at the onset of failure are almost identical to the initial values.

*5.2.1.3. Distribution of overburden pressure*. In the above section we discussed the variation of overburden pressure as a result of the cavity enlargement. In this section, we study the distribution of overburden pressure on the caprock at the onset of caprock failure.

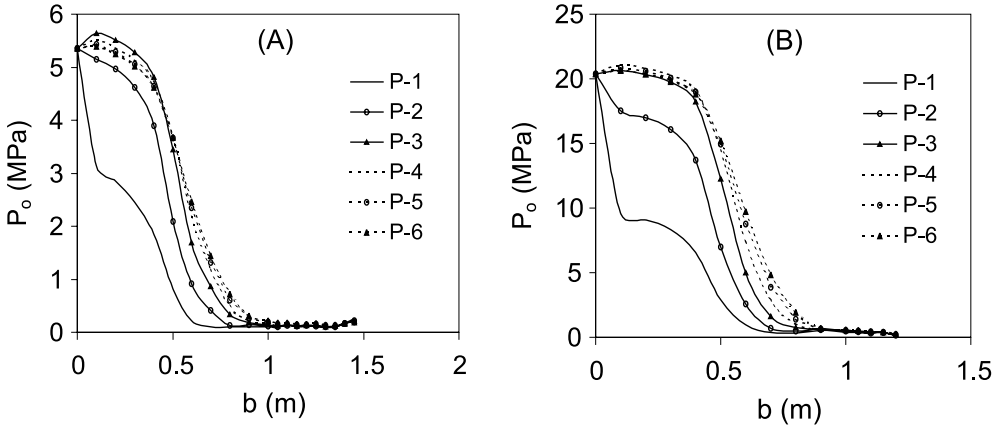


Fig. 14. Varition of overburden pressure with respect to the radius of cavity for Models A and B of Case 4.

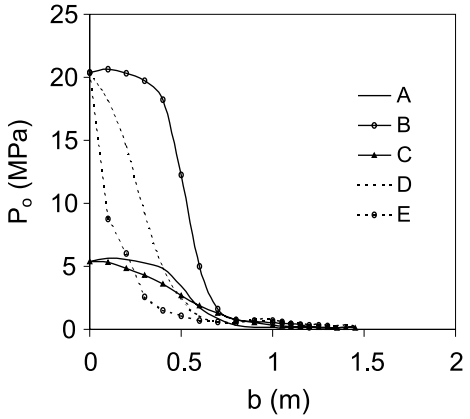


Fig. 15. Comparison of overburden pressure reduction under various conditions for Case 4.

Fig. 16 shows the lines of equal vertical stress around a cavity at a stage before the initiation of failure. In this figure, the saw-tooth edge represents the bottom of the caprock which has been affected by the removal of the elements that had undergone tensile failure. As shown in the figure, the vertical stress decreases with reducing distance from the cavity. It is to be noted that the overburden pressure over the caprock is in fact the vertical stress acting between the caprock and the overlying soil. Based on the contour lines presented in the figure, one can appreciate the small magnitude of the overburden pressure and its variation over the caprock.

Fig. 17 shows the FLAC generated distribution of the overburden stress at the surface of the caprock. The results obtained from Eq. (14) are also shown by straight lines. As the curves presented in this figure show, the overburden pressure values for all cases are significantly smaller than the initial in situ vertical stress. The differences between FLAC and analytical results, albeit appreciable in this respect, have minimal impact on the final results as evidenced by the data presented in Tables 2–5. Nevertheless, for discussion purposes, it is worth pursuing this point as follows.

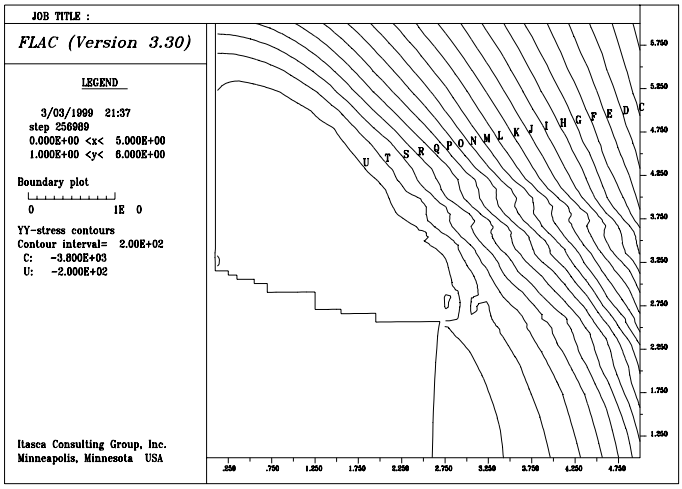


Fig. 16. Contour lines of vertical stress in the vicinity of the cavity for Model D of Case 3.

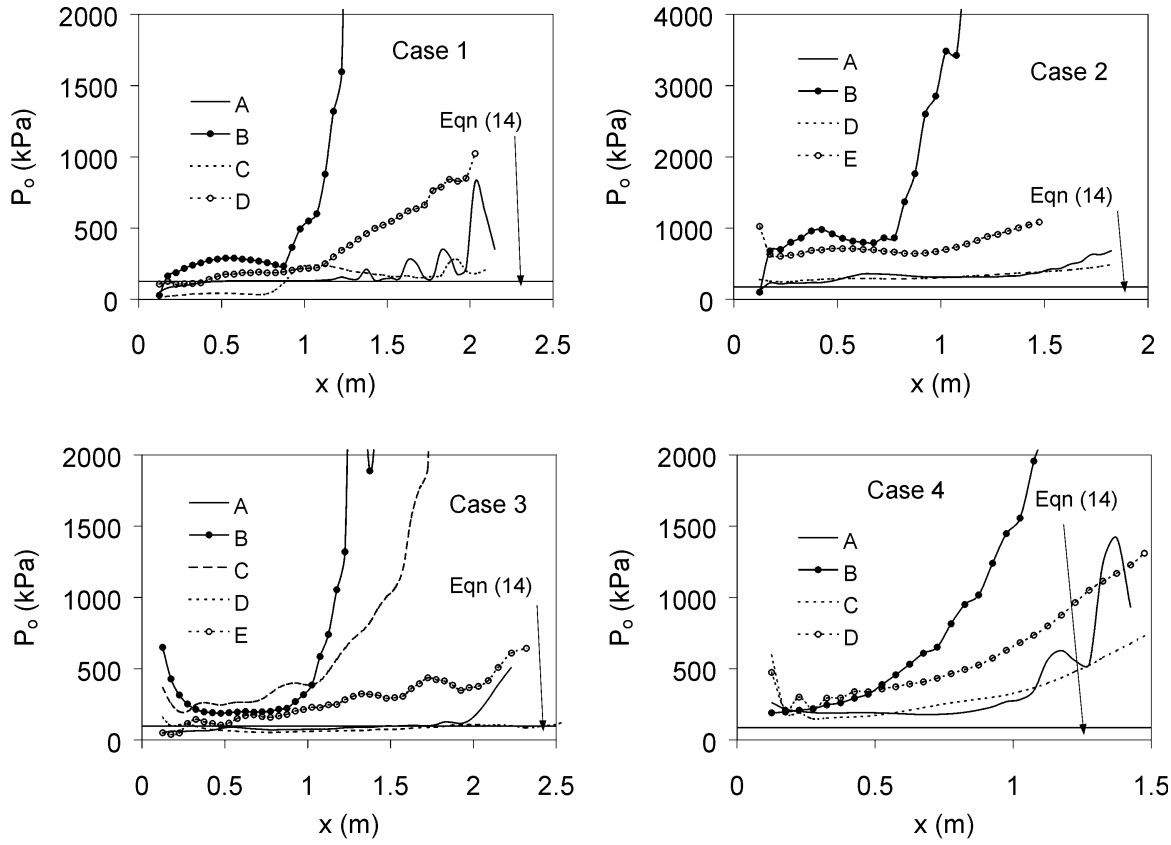


Fig. 17. Distribution of overburden pressure on the caprock.

In general, the overburden pressure increases with distance from the wellbore. This is because as the distance from the wellbore increases, the caprock deflection decreases. As reduction of the overburden pressure depends on the amount of deflection (recall curve abcd in Fig. 3), less reduction occurs when the distance from the wellbore increases. Applying a similar distribution of overburden pressure for the solution presented in Section 3 results in a considerable increase in compressive force in the dome at the supporting edge, which in turn induces failure in this area. However, none of the FLAC models produced this kind of failure. Caprock failure in all the FLAC models occurred at the wellbore lining. This is due to the fact that in FLAC models the caprock does not purely act as a compression dome. The behavior of the caprock in an FLAC model varies from a compression dome at the wellbore lining to a moment carrying element at the support. The presence of large horizontal compressive stresses at the support prevents initiation of tension cracks in this region resulting in a stronger section for the caprock at the support than at the wellbore lining. As the magnitude of stresses at the wellbore lining is mainly dependent on the magnitude of overburden pressure at the proximity of the wellbore, the increase in overburden pressure at the support practically does not have a significant effect on the caprock failure. Therefore, as adopted in our analytical method, the assumption of a uniformly distributed load over the caprock does not compromise the credibility of the final solution.

Another issue worth considering is the increase of overburden pressure within the close proximity of the wellbore in some models. This behavior is due to the high stress confinement at the wellbore lining. The

$x$-direction constraint at the wellbore lining for the overlying soil is the main contributor to confinement stress. To quantify this, we examine Model D of Case 4, wherein the overburden pressure in the adjacent element to the wellbore lining at one stage before failure was 473.9 kPa. This stress dropped to 245.9 kPa when the model was analyzed with no $x$-direction constraint for the overlying soil at the wellbore (Model E). The other source of the soil confinement is the caprock. In fact, in the FLAC models the elements representing the soil in contact with the caprock have common nodes with the elements representing the caprock. As the caprock is significantly stiffer than the soil, the common nodes have relatively small displacement in the $x$ direction. As such, an unrealistic confinement is reproduced. In practice, the amount of the confinement is significantly smaller. This is due to the fact that a full constraint in the $x$-direction does not prevail at the wellbore lining and the overlying soil can slide on the caprock. As a result, the true distribution of the overburden pressure is uniform or gradually decreasing near the wellbore lining.

In light of the above, we proceed to compare the relatively flat part of the stress distribution curves close to the wellbore with the values obtained from Eq. (14). As the figure shows, the values obtained from Eq. (14) are, in general, smaller than the values obtained from FLAC. While this particular aspect of the analytical model is on the unsafe side, this should not be alarming as the proposed analytical model was not intended to capture every detail of the whole system realistically. Our main objective was to develop a simple-to-use analytical model that is reliable for practical applications. The applicability of the proposed method for its intended use has been validated by the results presented in Tables 2–5. Therefore, the underestimation of the overburden pressure alone does not imply that the entire method is unsafe. Also, as was discussed earlier in this section, representing the caprock by a compression dome, in general, leads to an underestimation of the caprock strength. In view of this, had Eq. (14) been adjusted in such a way to yield larger values for the overburden pressure, the proposed analytical method would unreasonably underestimate the true cavity radius at the onset of failure.

Very briefly, some of the other points worth mentioning are

- There is a considerable amount of friction between the caprock and the overlying soil that helps the stability of the caprock. This effect is not considered in the proposed analytical method,
- Figs. 14 and 15 show some fluctuation in the magnitude of the overburden pressure as the cavity size increases. This is a numerical artifact and not a phenomenon one would expect to see in practice. The fluctuation in FLAC is probably due to failure in reaching a complete static equilibrium when the next column of soil is removed. For example, it was noticed that in some cases, the overburden pressure was increasing when the failure occurred. On the basis of this, it is reasonable to assume that some of the failure occurred under an oscillating condition. It is, therefore, possible that some of the cavity radii predicted by FLAC could be slightly different from the values that would have been obtained under an ideal static condition.
- In Fig. 17, the lines representing Eq. (14) are based on the failure radii determined from the analytical method.

## 6. Summary and conclusions

An analytical method is developed for determining the stability of a hard stratum (referred to as caprock) overlying a cylindrical cavity around a wellbore. Practical application of the proposed method is to oil and gas recovery projects that often have to consider the stability of the reservoir during the drilling and production phase. The dilemma faced by the industry is whether to allow sanding (or formation instability) to occur until a stable condition is reached or to prevent sanding altogether. The problem with the latter is that it is expensive to install and maintain sand exclusion systems and moreover, such systems tend to significantly compromise the long-term productivity of a well as they inevitably become plugged to some

extent. To permit sand production, it is critical to ensure that a stable condition would eventually prevail, that is, sand production will terminate. This requires containing sanding to the reservoir layer (basically lateral propagation of the sand failure) and preventing production of the overlying material. In this regard, only reservoirs that are overlain by a relatively competent caprock can be considered for this mode of wellbore completion. It is, therefore, beneficial to have an easy to use and reliable model that can be readily applied to field problems for assessing the integrity of the caprock under various plausible scenarios.

The proposed method can be used to assess the safety factor for a caprock under various conditions and the maximum cavity radius that can be sustained prior to its collapse. In the proposed method, the caprock is considered to behave as a structural element carrying the overburden pressure and its own weight. The proposed method is comprised of two basic operations: (1) estimation of the overburden pressure, and (2) computation of the caprock response.

For the estimation of the overburden pressure at the onset of failure, it is assumed that a cylindrical plastic region develops above the caprock within which the vertical stress decreases with depth. The minimum vertical stress between the caprock and the plastic region required for the stability of the overlying soil is assumed to be the overburden pressure at the onset of failure. We used two different assumptions for the magnitude of the shear stress on the circumference of the assumed plastic region, and accordingly derived two different (Eqs. (9) and (14)) for the overburden pressure. These equations are not a function of the magnitude of the in situ vertical stress as the caprock is assumed, rather realistically, to be at some considerable depth below the surface (typical reservoirs are generally hundreds of meters below the surface). The values of the overburden pressure from these equations become equal for the condition of $\phi \cong 40^{\circ}$. However, as the behavior of Eq. (14) is considered to be more realistic, we used this equation for estimating the overburden pressure of the case studies in Section 5.

To compute the caprock response, the solution proposed assumes the tensile strength is negligible and that the stability is governed by the strength of a compression dome formed within the caprock.

To validate the proposed analytical method, we used a commercial finite difference program called FLAC. Considering the fact that the numerical and analytical solutions follow a very different path in terms of assumptions embodied, comparison of the results obtained is surprisingly favorable. While in general the analytical solutions tend to be on the conservative side, the overall trends are consistent. The findings from this comparison are most encouraging in confirming that most of the assumptions made and the rationale used are fundamentally correct and field applicable. Some of the key points in this regard include the vertical (overburden) stress imposed on the caprock in the vicinity of the wellbore that reduces considerably as a result of wellbore drilling and any enlargement of the cavity size. The magnitude of reduction increases with the cavity radius, caprock deflection and the overlying soil stiffness. The overburden stress at the onset of failure is significantly smaller than the in situ vertical stress.

The main differences between the proposed analytical and numerical solutions are

- FLAC does not exhibit a uniform distribution of the overburden stress as assumed in the analytical model. In FLAC, as it would be expected, the overburden stress increases with distance from the wellbore.
- While the magnitudes of the overburden pressure obtained from the finite difference and analytical solution (Eq. (14)) are reasonably close, the analytical results, in general, are smaller.
- The solution presented for the caprock behavior underestimates the caprock strength. This, however, tends to balance the differences arising from the greater reduction in the overburden stress and the assumption of uniform overburden stress distribution.

In spite of the above noted differences, the proposed analytical model is considered suitable for practical applications. As with any analytical model some simplifying assumptions had to be made to achieve a closed form solution, however, as it has been shown here, the influence of these assumptions on the final result has been small and well within the range of accuracy that can be comfortably tolerated in practice.

## References

Adler, L., Sun, M., 1968. Ground Control in Bedded Formations, Bulletin 28, Research Division, Virginia Polytechnic Institute.

Baker, R.M., Hatt, F., 1972. Joint Effects in Bedded Formation Roof Control. New Horizons in Rock Mechanics. Proc. 14th US Symp. Rock Mech., ASCE, New York, pp. 247–261.

Beer, G., Meek, J.L., 1982. Design Curves for Roofs and Hanging Walls in Bedded Rocks based on Voussoir Beam and Plate Solution. Trans. Instn. Min. Metall. 91, A18–22.

Evans, W.H., 1941. The strength of undermined strata. Trans. Instn. Min. Metall. 50, 475–532.

FLAC Users Manual 1996, Itasca Consulting Group, Inc., 708 South Third Street, Suit 310, Minneapolis, Minnesota 55415, USA.

Florence, A., Schwer, L.E., 1978. Axisymmetric compression of a Mohr–Coulomb medium around a circular hole. Int. J. Numer. Anal. Meth. Geomech. 2, 367–379.

Hoek, E., Brown, E.T., 1980. Underground Excavations in Rock. The Institution of Mining and Metallurgy, London.

Meyerhof, G.G., Adam, J.I., 1968. The Ultimate Uplift Capacity of Foundations. CGJ Ottawa 5 (4), 225–244.

Obert, L., Duvall, W.I., 1967. Rock Mechanics and the Design of Structures in Rock. Wiley, New York.

Palmer, I.D., Mavor, M.J., Siedle, J.P., Volz, R.F., 1993. Openhole Cavity Completion in Coalbed Methane Wells in San Juan Basin. SPE, Journal of Petroleum Technology, November issue, 1072–1080.

Risnes, R., Bratli, R.K., Horsrud, P., 1982. Sand Stress Around a Wellbore. Society of Petroleum of AIME (SPE), pp. 883–898.

Spangler, M.G., Handy, R.L., 1971. Soil Engineering, third ed. Intext Educational Publishers, New York.

Sterling, R.L., 1980. The Ultimate Load Behavior of Laterally Constrained Rock Beams. The State of the Art in Rock Mechanics. Proc. 21st US Symp. Rock Mech., University of Missouri, Rolla, pp. 553–542.

Timoshenko, S., 1940. Theory of Plates and Shells. McGraw Hill, New York.

Ugural, A.C., 1981. Stress in Plates and Shells. McGraw-Hill, New York.

Vaziri, H., Palmer, I., Wang, X., 1997a. Wellbore Completion technique and geotechnical parameters influencing gas production. Canadian Geotech. J. 34, 87–101.

Vaziri, H., Phillips, R., Hurley, S., 1997b. Physical modelling of sand production. Int. J. Rock Mech. Min. Sci. 34 (3–4), Paper no. 323.

Vaziri, H., Wang, X., Palmer, I., Khodaverdian, M., McLennan, J., 1997c. Back Analysis of coalbed strength properties from field measurements of wellbore cavitation and methane production. Int. J. Rock Mech. Mining Geomech. Abst. 34 (6), 963–978.

Vaziri, H., Thallak, S., Phillips, R., 1998. Investigation of Sand Production Mechanisms Resulting in Enhanced Cold Production. ISSMFE Centrifuge 98, Tokyo, Japan.

Yeung, K.C., 1995. Cold Flow Production of Crude Bitumen at the Burnt Lake Project, Northeastern Alberta, Canada. 6th UNITAR Int. Conf. on Heavy Crude and Tar Sands, Houston, Feb. 12–15. p. 31.

Wang, Y., Dusseault, M.B., 1994. Stress around a circular opening in an elastoplastic porous medium subjected to repeated hydraulic loading. Int. J. Rock Mech. Sci. Geomech. Abstr. 31 (6), 597–616.

Wilkins, M.L., 1964. Fundamental method in hydrodynamics. Meth. Computat. Phys. 3, 211–263.